Journal of Polymers and the Environment (2024) 32:164–181
https://doi.org/10.1007/s10924-023-02988-7

ORIGINAL PAPER

Versatile Multi-Network Hydrogel of Acrylamide, Sodium Vinyl Sulfonate, and N,N′-Methylene Bisacrylamide: A Sustainable Solution for Paracetamol Removal and Swelling Behavior

Seda Melis Süren[1] · Rumeysa Tutar[1] · Cemal Özeroğlu[1] · Selcan Karakuş[1]

Accepted: 5 July 2023 / Published online: 20 July 2023

Abstract
The multi-network hydrogel synthesized using a novel combination of acrylamide and sodium vinyl sulfonate as monomers, along with N,N′-methylene bisacrylamide as a crosslinking agent, exhibits promising potential for applications in wastewater treatment and drug delivery systems. In addition to evaluating the chemical and thermal properties, the swelling behavior of the hydrogels was examined. Furthermore, the findings from the study of paracetamol adsorption onto the multi-network hydrogel were examined utilizing a variety of adsorption isotherms and kinetic models. The results demonstrate that the hydrogel with a swelling equilibrium value of 265.78 g H_2O/g dry gel has considerable potential for the removal of paracetamol from aqueous solution, with the pseudo-second-order kinetic model offering an outstanding fit to the experimental data. This work contributes to the development of potential and sustainable materials for environmental and biomedical applications.

Keywords Hydrogels · Vinylsulfonic acid sodium salt · Acrylamide · Adsorption · Paracetamol · Drug delivery · Wastewater treatment · Multi-network

Introduction

Hydrogels are a type of polymer material that can absorb and hold large amounts of water without losing their structure [1–3]. The interconnected pores formed by the polymer chains that make up hydrogels allow water to flow in and out freely, while the polymer chains themselves swell and expand as they absorb water [1, 4]. This property creates a sponge-like substance capable of holding many times its weight in liquid. The unique properties of hydrogels make them valuable in a range of industries, including medicine, agriculture, and environmental engineering [5–8].

In medicine, hydrogels are used as scaffolds for tissue engineering, wound dressings, and drug delivery systems [9–11]. The ability of hydrogels to gradually release drugs over time can increase their effectiveness and reduce side effects [12, 13]. In agriculture, hydrogels can be applied to soil to improve water retention and nutrient availability. They can also help reduce the amount of water needed for irrigation, making them a sustainable option for farming. In environmental engineering, hydrogels can be utilized to filter toxins out of water and soil, providing a solution for water purification and soil remediation [14–16]. Particularly in the biomedical industry, hydrogels have demonstrated their potential as scaffolds for tissue engineering [17, 18], controlled release systems for drugs [19, 20], and wound dressings [19, 21]. By mimicking the natural environment of cells, hydrogels can support cell growth and regeneration, making them a promising material for tissue engineering applications. Overall, the versatility and unique properties of hydrogels make them a valuable material with broad applications in various industries [22].

The swelling theories of hydrogels aim to explain the behavior of hydrogels during the process of swelling and deswelling by considering the chemical and physical interactions between the hydrogel and its environment [23–25]. In addition, modeling nonlinear flexibility is an important research topic that helps to better understand the mechanical

✉ Cemal Özeroğlu
ozeroglu@iuc.edu.tr

✉ Selcan Karakuş
selcan@iuc.edu.tr

[1] Department of Chemistry, Faculty of Engineering, Istanbul University-Cerrahpaşa, Avcılar, 34320 Istanbul, Turkey

behavior of hydrogels produced under different loading conditions [26]. These concepts are particularly important for pH and temperature-responsive hydrogels, as they may exhibit reversible changes in their physical and chemical properties, such as swelling and deswelling, in response to changes in temperature and pH levels [27–29]. The development of several biomaterials, in particular controlled drug release systems, has benefited greatly from the use of these hydrogels. Hydrogels can be used for drug delivery by modifying their chemical composition in response to changes in temperature or pH. This allows for precise control over the rate of drug dissolution and dosage [30, 31]. For example, a hydrogel can be designed to swell at specific pH levels and release drugs that are encapsulated within it. Furthermore, these hydrogels can respond to changes in temperature, enabling further control of the drug release rate. The capacity of hydrogels to carry drugs is directly correlated with their adsorption abilities. Drugs can be released from hydrogels with high drug delivery capacity in a controlled and prolonged route, improving therapeutic effectiveness and minimizing side effects. By improving their solubility and stability, hydrogels can also enhance their bioavailability and protect pharmaceuticals from degradation. In recent years, the demand for effective and economical materials for environmental and medicinal applications has increased dramatically. Due to their unique characteristics, including high water content, biocompatibility, and excellent capacity for medication delivery and pollutant removal, hydrogels have become recognized as a promising class of materials.

The hydrogel's versatile multi-network structure renders it highly advantageous for a range of applications, including swelling hydrogels and wastewater treatment. This structure seamlessly integrates the favorable properties of a highly crosslinked hydrophilic network, such as superior water absorption and retention, with the swelling capacity and selective permeability offered by a less crosslinked hydrophobic network. By combining functionality and versatility, this hydrogel exhibits tremendous potential for diverse applications. In this study, a versatile multi-network hydrogel of acrylamide (AAm), sodium vinyl sulfonate (SVS), and N,N′-methylene bisacrylamide (MBAA) was synthesized and characterized, with potential applications in wastewater treatment and drug delivery systems. The hydrogel's chemical and thermal characteristics were evaluated, and the swelling behavior was examined.

Paracetamol, a commonly used drug for alleviating pain and reducing fever, raises concerns when found in wastewater and the environment due to its possible negative impacts on aquatic ecosystems and human well-being. Traditional methods of treating wastewater often prove insufficient in eliminating paracetamol, resulting in its continued presence and persistence in the environment. Hydrogel shows great promise for addressing the issue of paracetamol contamination in wastewater and the environment. In this study, we examined the capacity of hydrogel to adsorb paracetamol using different adsorption isotherms and kinetic models. The findings revealed that the hydrogel exhibited significant potential for effectively removing paracetamol from aqueous solutions, with the pseudo-second-order kinetic model demonstrating a strong fit to the experimental data. These results have significant implications for the development of sustainable materials in the fields of biomedicine and environmental conservation, offering a potential solution to mitigate the adverse effects of paracetamol on aquatic ecosystems and human health.

Material and Methods

Material

Acrylamide (AAm) (purity: 98% and molecular weight: 71.08 g/mol), cerium(IV) sulfate tetrahydrate (purity: 98% and molecular weight: 404.3 g/mol), sulfuric acid (H_2SO_4) (purity: 98% and molecular weight: 98.08 g/mol), and ethylene diamine tetraacetic acid tetra sodium salt (EDTANa4) (molecular weight: 380.17 g/mol) were obtained from Merck Company (Germany). N,N′-methylene bisacrylamide (MBAA) (purity: 99%, molecular weight: 154.17 g/mol) were obtained from Fluka Company (Germany). Mercaptosuccinic acid (MSA) (purity: 99% and molecular weight: 150.15 g/mol), sodium vinyl sulfonate (SVS) (purity: 99% and molecular weight: 130.10 g/mol), and Paracetamol (Par, British pharmacopoeia reference standard and molecular weight: 151.163 g/mol) were obtained from Sigma Aldrich Company (Germany). All chemicals were analytical grade and used as received without further purification. By utilizing distilled water in the swelling experiments, the potential for changes in water composition was effectively minimized, enabling a more controlled and reliable assessment of the hydrogel's swelling behavior. This deliberate choice aimed to eliminate any interference from impurities or other extraneous factors, ensuring that the observed swelling properties could be accurately attributed solely to the inherent characteristics of the hydrogel.

Preparation of Hydrogels

The multi-network hydrogel, synthesized using a novel combination of acrylamide (AAm) and sodium vinyl sulfonate (SVS) as monomers, along with N,N′-methylene bisacrylamide (MBAA) as a crosslinking agent, exhibits promising potential for applications in wastewater treatment and drug delivery systems. The synthesis process involved several steps: initially, 1.415 g of cerium(IV) sulfate tetrahydrate salt was added to 1.4 mL of H_2SO_4, and the volume was

increased to 100 mL with distilled water. Subsequently, a solution containing 4.308 g of AAm, 7.806 g of 25% SVS, 0.1168 g of MBAA, 0.0225 g of MSA, and 0.225 g of EDTANa4 salt was dissolved in 100 mL of distilled water. Finally, 2 mL of the cerium solution was added, resulting in the formation of the versatile multi-network hydrogel composed of AAm, SVS, and MBAA.

Characterizations

Fourier transform infrared spectroscopy (FTIR) is a technique used to analyze the chemical composition of a sample by measuring the absorption or transmission of infrared radiation. In this case, the hydrogel samples were analyzed using a Thermo Scientific Nicolet 380 spectrometer in the frequency range of 400–4000 cm^{-1}. The KBr disk method involves mixing a small amount of the hydrogel sample with powdered KBr and compressing it into a disk for analysis. Thermal gravimetric analysis (TGA) is a technique used to study the thermal behavior of a material by measuring its weight as it is heated or cooled under controlled conditions. In this study, the prepared hydrogel samples were dried, ground to a powder, and placed in a platinum crucible. The sample was heated from 0 to 600 °C under nitrogen gas with a heating rate of 10 °C/min, and the changes in mass of the samples were recorded. The resulting data can be used to determine the thermal stability of the hydrogel, which can help assess its potential for various applications. Scanning electron microscopy (SEM) ((FEI QUANTA 450 Model) was employed to characterize both the hydrogel and paracetamol-loaded hydrogel, providing detailed insights into their morphological characteristics. The SEM analysis was performed at a working distance of 6–10 mm, a pressure range of 0–130 Pa, and an applied voltage of 7–10 kV under low vacuum conditions.

Calculation of Swelling Kinetic Model Parameters

Hydrogels are known for their ability to swell and absorb large amounts of water. To better understand this behavior, a study was conducted to investigate the swelling kinetics of hydrogels through gravimetric measurement [32]. Measurements were conducted at various time intervals, ranging from 2 to 48 h, using dried hydrogels to ascertain the swelling rate of the hydrogel. The swelling experiments on the hydrogel were conducted three times, resulting in consistent and reliable results. The study also examined the effects of crosslinker concentrations at different temperatures on the swelling properties of the hydrogels. Swelling ratios were calculated using two equations, with S_t and S_{eq} values representing the swelling at a specific time and at equilibrium, respectively (Eqs. 1–2) [33]. This calculation provides valuable insights into the swelling behavior of hydrogels, which could have potential applications in various fields such as adsorption and drug delivery systems.

$$S_t = \frac{m_t - m_o}{m_o} \tag{1}$$

$$S_{eq} = \frac{m_{eq} - m_o}{m_o} \tag{2}$$

The properties of hydrogels, which are materials that can absorb considerable amounts of water, vary depending on how much water they absorb in. Initially developed, hydrogels are frequently in a dehydrated or "dry"structure. The variable m_o represents the dry mass of a hydrogel sample and is used as a standard for calculating the hydrogel's water uptake. The mass of the hydrogel grows as water is absorbed, and at a specific time point (t), the swelling mass of the hydrogel is indicated by the variable mt. The variable m_{eq} stands for the swelled mass of the hydrogel at equilibrium, or the point at which the hydrogel can no longer absorb any more water. Swelling ratios, such S_t and S_{eq}, are used to describe the amount of water the hydrogel is holding at various periods. While S_{eq} denotes the quantity of water contained by 1 g of dry hydrogel at equilibrium, S_t denotes the amount of water held by 1 g of dry hydrogel at a certain time point (t). These ratios are crucial indicators of the hydrogel's capacity to take in and retain water, and they can be beneficial in applications including the delivery of drugs, tissue engineering, and wound healing. The developed hydrogels' swelling kinetic models confirmed their water absorption abilities and provided evidence for applying the Voigt kinetic model (Eq. 3) in the presence of deionized water to identify the process of water absorption into the hydrogel. Equation (4) provided the Voigt model's linear graph. The slope of the linear graph, represented as $(-1/\tau)$, was calculated with the intention of determining the kinetic rate parameter (τ) [32].

$$S_t = S_{eq}(1 - e^{-\frac{t}{\tau}}) \tag{3}$$

$$Ln(1 - \frac{S_t}{S_{eq}}) = -\frac{1}{\tau}t \tag{4}$$

By understanding the kinetic and diffusion properties of the hydrogel, researchers can optimize its design for biomedical applications.

Calculation of Adsorption of Paracetamol

Paracetamol is a widely used pain reliever commonly found in pharmaceutical formulations. In recent years, there has been increasing interest in using hydrogels as adsorbents for paracetamol due to their unique physical and chemical

properties. In this study, the adsorption mechanism of paracetamol using a versatile multi-network AAm/SVS/MBAA hydrogel was investigated by calculating its kinetic models, isotherms, and thermodynamic properties. Thermodynamic parameters such as kinetic model parameters, enthalpy, entropy, and Gibbs free energy change were calculated to explain the adsorption process and to understand the nature of adsorption. This study showed that the adsorption of paracetamol to hydrogels is a complex process influenced by various factors such as temperature, pH, and concentration. Overall, the development of effective paracetamol adsorption systems using hydrogels has the potential to offer a promising alternative for the removal of this drug from aqueous solutions. Table 1 summarizes the kinetic models, isotherms, and thermodynamic calculations used in this study [34–38].

C_o represents the initial concentration (mg/L) of paracetamol solution, while C_e represents the equilibrium concentration (mg/L) of paracetamol after adsorption. V represents the volume (ml) of the solution and m represents the amount of absorbent used. K_d represents the distribution coefficient.

$$R = 8.314\,J/(K \cdot mol)$$

For the measurement of paracetamol on the hydrogel, 0.05 g of dry hydrogel was weighed for each adsorption experiment and allowed to swell in distilled water for 1 week until it reached the equilibrium swelling value. In the paracetamol adsorption process on the hydrogel, each swollen hydrogel was mixed with 10 mL of a solution containing different concentrations of paracetamol. The effects of various paracetamol concentrations, adsorption time, and temperature on the adsorption measurements of paracetamol from aqueous solutions were investigated. Spectrophotometric measurements were used to measure the absorbance values at 243 nm before and after adsorption. The adsorption parameters and adsorption energy were determined by applying the adsorption data obtained at different paracetamol concentrations to the Freundlich, Langmuir, and Dubninin-Radushkevich (D-R) isotherms. The suitability of the adsorption data obtained over time was investigated using the modified Freundlich, Elovich, pseudo-first order kinetic, and pseudo-second order kinetic models, and the adsorption rate parameters were determined. The thermodynamic parameters (ΔH^0, ΔS^0, and ΔG^0) were calculated using the adsorption data obtained at different temperatures.

Results and Discussion

Characterization of Multi-Network SVS-AAm-MBAA Hydrogel

The results of the FTIR analysis for the hydrogels showed the characteristic functional groups of the hydrogel multi-networks. FT-IR spectra of hydrogels synthesized with AAm: 0.06 mol, SVS: 0.015 mol, and MBAA: 7.5×10^{-4} mol (red line) and AAm: 0.075 mol, SVS = 0 mol, and MBAA: 7.5×10^{-4} mol (blue line) hydrogels were shown in Fig. 1, with the characteristic functional groups identified.

For the AAm-MBAA hydrogel, the FTIR spectra showed absorption peaks at 3500–3300 cm^{-1} (stretching bands of N–H and O–H bonds), 2918 cm^{-1} (–CH_3 groups), 2926 cm^{-1} (–CH_2 groups), and 1649 cm^{-1} (amide I) [39, 40]. For the SVS-AAm-MBAA hydrogel, the FTIR spectra showed absorption peaks at 3500–3300 cm^{-1} (stretching bands of N–H and O–H bonds), 2918 cm^{-1} (–CH_3 groups), 2926 cm^{-1} (–CH_2 groups), 1649 cm^{-1} (amide I), 1400 cm^{-1} (SO_3 asymmetric stretch), and 1036 cm^{-1} (sulfonate group).

Table 1 Kinetic models, isotherms, and thermodynamic calculations

Model	Equation	Parameters
Freundlich isotherm	$q_e = K_F C_e^{1/n}$	q_e: Amount of adsorbed paracetamol (mmol/g), K_F: Freundlich adsorption constant, C_e: Equilibrium concentration (mol/L), and n: Freundlich adsorption exponent
Langmuir isotherm	$Ce/qe = 1/(b\,q_{max}) + Ce/q_{max}$	b: Langmuir adsorption isotherm constant
Dubinin-Radushkevich isotherm	$\varepsilon = R\,T\ln(1 + 1/Ce)$	ε: Polanyi potential
Modified freundlich kinetic model	$\ln q_t = \ln a + b\,\mathrm{Int}$	a and b: Modified Freundlich rate constants
Elovich kinetic model	$q = (1/\beta)\ln(\alpha\beta) + (1/\beta)\ln(t)$	α: Initial adsorption rate, β: Desorption constant
Pseudo-first order kinetic model	$\ln(q_e - q_t) = \ln q_e - kt$	
Pseudo-second order kinetic model	$\frac{t}{q_t} = \frac{1}{kq_e^2} + \frac{1}{q_e}t$	k: Pseudo-second order rate constant
	$K_d = \frac{C_0 - C_e}{C_e} \times \frac{V}{m}$	
	$\ln K_d = -\frac{\Delta H^0}{RT} + \frac{\Delta S^0}{R}$	
	$\Delta G^0 = \Delta H^0 - T\,\Delta S^0$	

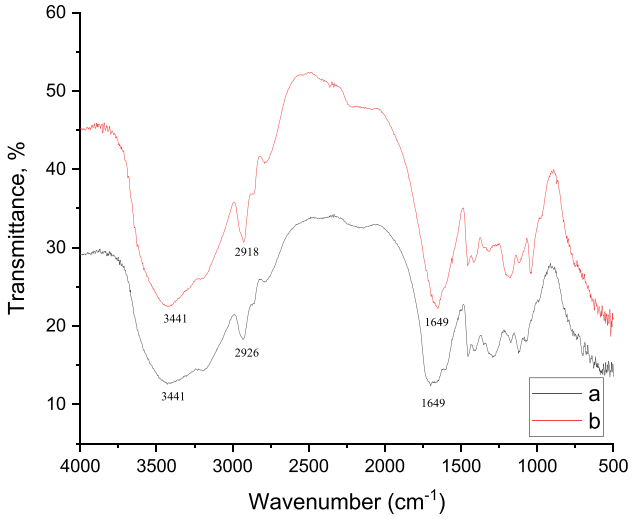

Fig. 1 FT-IR spectra of hydrogels synthesized with **a** multi-network SVS-AAm-MBAA hydrogel (AAm: 0.06 mol, SVS: 0.015 mol and MBAA: 7.5×10^{-4} mol (red line)) and **b** AAm-MBAA hydrogel (AAm: 0.075 mol, SVS = 0 mol and MBAA: 7.5×10^{-4} mol (blue line))

Figure 2 shows the TGA curves of the synthesized hydrogels, including (a) AAm-MBAA hydrogel (AAm = 0.075 mol, SVS = 0 mol, and MBAA: 7.5 × 10–4 mol; represented by the blue line), (b) multi-network SVS-AAm-MBAA hydrogel (AAm: 0.06 mol, SVS: 0.015 mol, and MBAA: 7.5 × 10–4 mol; represented by the red line). Additionally, SEM images of the pure AAm/SVS/MBAA hydrogel and the paracetamol-loaded AAm/SVS/MBAA hydrogel are presented. The results presented in Fig. 2**.e** show the UV–Visible spectrum of a 20 ppm paracetamol aqueous solution (pH 6.6).

Thermogravimetric analysis (TGA) is a technique that analyzes the change in weight of a material as a function of temperature or time, conducted under controlled settings. In this study, the thermal stability of two hydrogels, namely AAm-MBAA and SVS-AAm-MBAA hydrogel, was examined using TGA results. Figure 2a, b illustrates the TGA curves for both hydrogels, depicting the variation in weight as the temperature increases. Through the examination of these TGA curves, the thermal stability of the hydrogels across a wide temperature range of 20 to 800 °C can be determined. The TGA study of the prepared AAm-MBAA and SVS-AAm-MBAA hydrogels was shown in Fig. 2a, b as a percentage weight loss versus temperature. The TGA graph of the AAm-MBAA hydrogel demonstrates weight reduction occurring in three distinct phases (Fig. 2a). The weight loss during the first stage, which ranged from 0 to 149 °C, amounted to 11.4%, primarily attributed to the elimination of absorbed water. In the second stage, spanning from 149 to 447 °C, a weight loss of 66.3% was observed, indicating intermolecular dehydration processes taking place. In the third stage, which occurred between 447 and 669 °C, a weight loss of 22.3% was observed, indicating the breaking of crosslinks between various polymer chains. Conversely, the TGA graph of the multi-network SVS-AAm-MBAA hydrogels exhibited a similar three-stage weight loss process (Fig. 2b). The first stage, spanning from 0 to 152 °C, resulted in a 12.8% weight reduction. In the second stage, which occurred between 152 and 424 °C, a weight loss of 56.6% was observed. The third stage, ranging from 424 to 698 °C, resulted in a weight loss of 30.6%. These findings demonstrated that there are three distinct phases of weight loss, occurring between 0 and 149 °C (elimination of absorbed water), 149 °C and 447 °C (intermolecular dehydration processes), and 447 °C and 669 °C (breaking of crosslinks between polymer chains), respectively. The prepared AAm-MBAA and SVS-AAm-MBAA hydrogels displayed similar three-stage breakdown patterns, yet the SVS-AAm-MBAA hydrogels exhibited a higher weight loss compared to the AAm-MBAA hydrogels, along with a slightly higher thermal decomposition temperature. These TGA results provided clear evidence of the exceptional thermal stability of the multi-network SVS-AAm-MBAA hydrogels, as indicated by the low percentage of weight loss. Furthermore, Khosravi et al. conducted an extensive investigation into the thermal properties of chitosan-g-poly(acrylic acid-co-acrylamide) hydrogel in literature, emphasizing its potential as a highly efficient matrix for drug delivery [41]. Through a comparison of the TGA thermogram of the hydrogel with our findings, it became apparent that the decomposition process exhibited distinct weight loss zones: the first zone (30–190 °C) resulted in a 7.1% loss attributed to moisture and volatiles, the second zone (190–321 °C) displayed a 20.7% loss, and the third zone (321–500 °C) showed a 29.4% loss, representing the loss of grafted chains and fragmentation of the backbone, respectively. In conclusion, the experimental findings established the hydrogel's high thermal stability, emphasizing its suitability for a wide range of applications.

The SEM technique was employed to study the surface morphology of both the pure AAm/SVS/MBAA hydrogel and the paracetamol-loaded AAm/SVS/MBAA hydrogel. The SEM images (Fig. 2c) provided visual evidence of a partially smooth surface in the hydrogel, indicating its overall homogeneity in terms of structure. The SEM results provide clear evidence that paracetamol adsorption alters the surface properties of the AAm/SVS/MBAA hydrogel (Fig. 2d). A distinct difference in surface roughness is observed between the paracetamol-loaded hydrogel and the pure hydrogel in the SEM images. In contrast to the relatively smooth surface of the pure hydrogel, the presence of the drug induces changes that lead to a coarser or textured surface. This observation suggests an interaction between the drug molecules

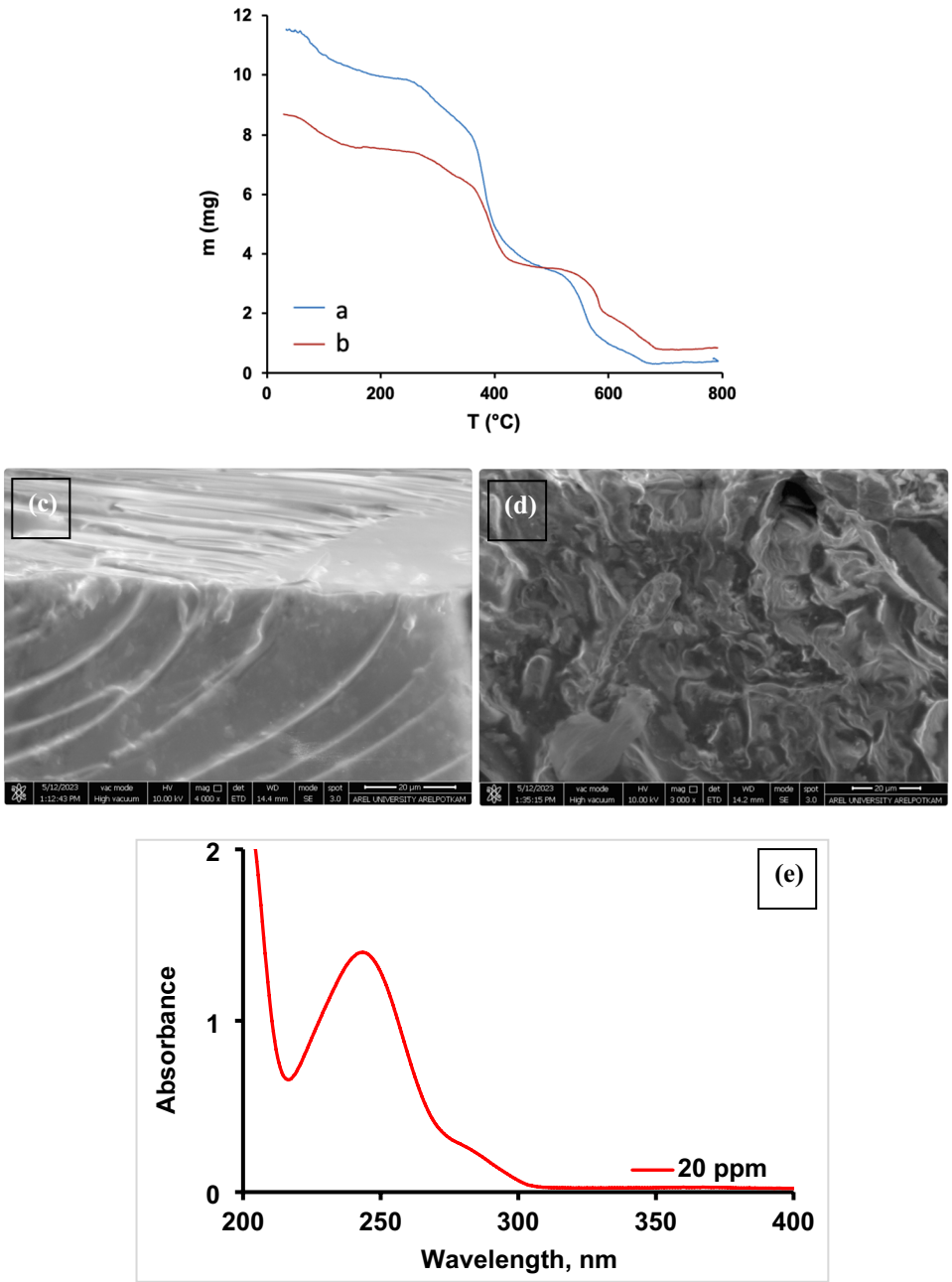

Fig. 2 TGA curves of synthesized with **a** AAm-MBAA hydrogel (AAm = 0.075 mol, SVS = 0 mol and MBAA: 7.5 × 10–4 mol (blue line)), **b** multi-network SVS-AAm-MBAA hydrogel (AAm: 0.06 mol, SVS: 0.015 mol and MBAA: 7.5 × 10–4 mol (red line), SEM images of **c** pure hydrogel, **d** drug loaded hydrogel, and **e** UV–Visible spectrum of 20 ppm parasetamol aqueous solution (Color figure online)

and the hydrogel matrix, potentially resulting in surface adsorption.

Swelling Profiles of Multi-Network SVS-AAm-MBAA Hydrogel

To determine the effect of different experimental conditions on the swelling properties of monomer/crosslinker ratio (AAm/MBAA: 25, 50, 100, 250, 1000 and 2000) and MBAA concentrations (3×10^{-3} mol, 1.5×10^{-3} mol, 7.5×10^{-4} mol, 3×10^{-4} mol, 7.5×10^{-5} mol, 5×10^{-5} mol and 3.75×10^{-5} mol) were investigated. In Fig. 3, swelling behavior of multi-network SVS-AAm-MBAA hydrogel with different crosslinker compositions (n_T/n_{MBAA}): (a) n_{AAm}: 0.075 mol and n_{SVS}: 0, (b) n_{AAm}: 0.069 mol, n_{SVS}: 0.006 mol n_T: 0.075 mol and n_{SVS}/n_{AAm}: 0.087, (c) n_{AAm}: 0.065 mol, n_{SVS}: 0.010 mol, n_T: 0.075 mol, and n_{svs}/n_{AAm}: 0.154, (d) n_{AAm}: 0.060 mol; n_{SVS}: 0.015 mol; n_T: 0.075 mol, and n_{svs}/n_{AAm}: 0.250, (e) n_{AAm}: 0.050 mol, n_{SVS}: 0.025 mol, n_T: 0.075 mol, and nsvs/n_{AAm}: 0.500, (f) n_{AAm}: 0.040 mol, n_{SVS}: 0.035 mol, n_T: 0.075 mol, and n_{svs}/n_{AAm}: 0.875, and (g) n_{AAm}: 0.035 mol, n_{SVS}: 0.040 mol,

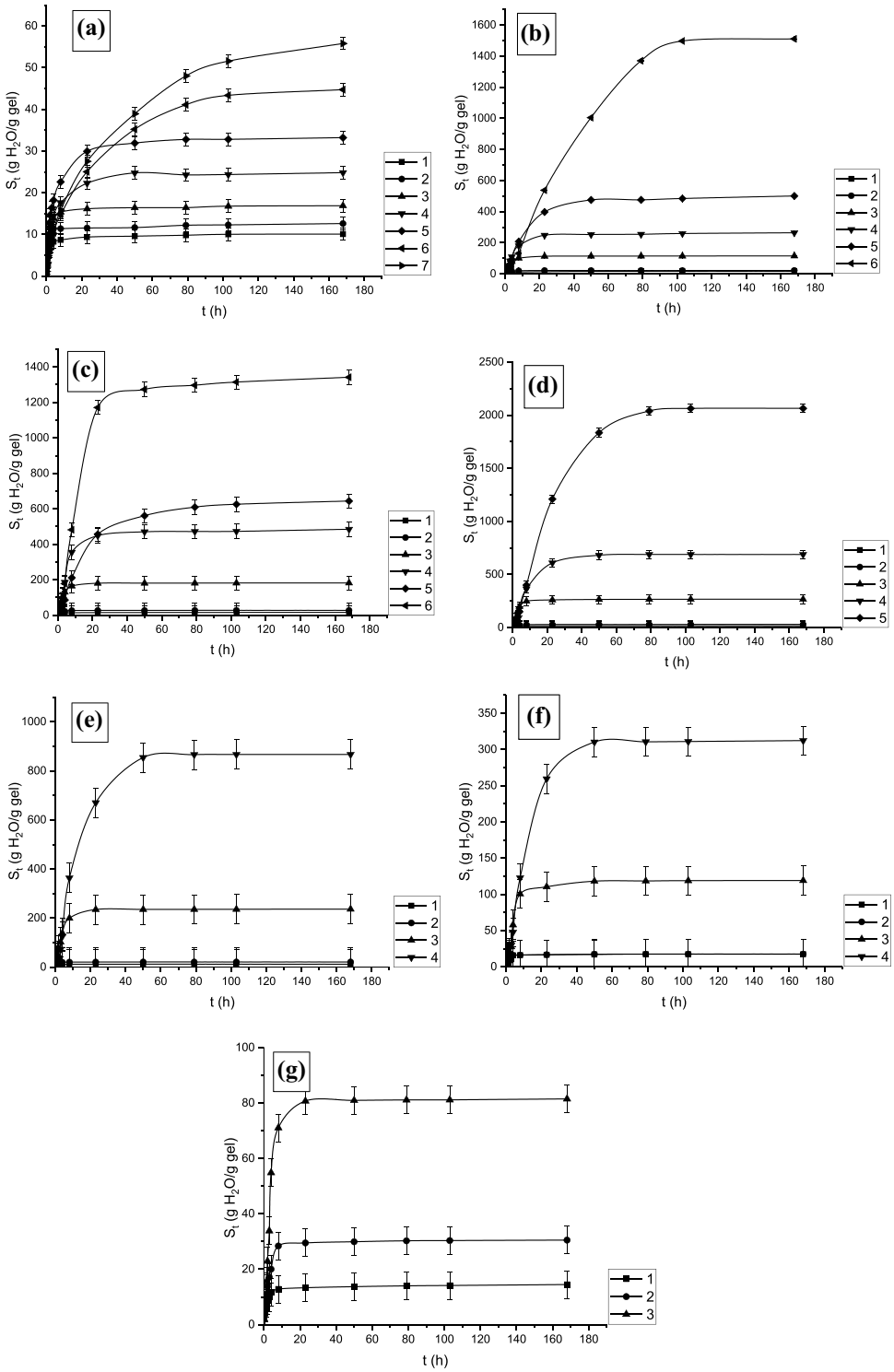

Fig. 3 Swelling behavior of multi-network SVS-AAm-MBAA hydrogel with different compositions (n_T/n_{MBAA}): **a** n_{AAm}: 0.075 mol and n_{SVS}:0, **b** n_{AAm}: 0.069 mol, n_{SVS}: 0.006 mol, n_T: 0.075 mol and n_{SVS}/n_{AAm}: 0.087, **c** n_{AAm}: 0.065 mol, n_{SVS}: 0.010 mol, n_T: 0.075 mol, and n_{svs}/n_{AAm}: 0.154, **d** n_{AAm}: 0.060 mol; n_{SVS}: 0.015 mol; n_T: 0.075 mol, and n_{svs}/n_{AAm}: 0.250, **e** n_{AAm}: 0.050 mol, n_{SVS}: 0.025 mol, n_T: 0.075 mol, and nsvs/n_{AAm}: 0.500, **f** n_{AAm}: 0.040 mol, n_{SVS}: 0.035 mol, n_T: 0.075 mol, and n_{svs}/n_{AAm}: 0.875, and **g** n_{AAm}: 0.035 mol, n_{SVS}: 0.040 mol, n_T: 0.075 mol, and n_{svs}/n_{AAm}: 1.143 (T: SVS + AAm)

n_T: 0.075 mol, and n_{svs}/n_{AAm}: 1.143, respectively (T: SVS + AAm) was given.

As seen from Fig. 3a, it was observed that the equilibrium swelling values of the hydrogels increased as the $n_{AAm/nMBAA}$ ratio increased. When the $n_{AAm/nMBAA}$ molar ratio was increased from 25 to 2000, it was observed that the equilibrium swelling value of the synthesized hydrogel in distilled water increased from 10.05 g H_2O/g gel value to 69.57 g H_2O/g gel value. In the polymerization reaction, different amounts of crosslinker (n_T/n_{MBAA}: 25–2000 ratios) were used to synthesize SVS-AAm copolymers at room temperature using the MSA-Ce(IV) initiator system,

with 0.069 mol of AAm and 0.006 mol of SVS. The time-dependent swelling curves of the obtained hydrogels in distilled water and their equilibrium swelling values are examined. In summary, the experimental results showed the relationship between the $n_{AAm/nMBAA}$ ratio and the equilibrium swelling values of hydrogels. It also provided details about the optimization design of SVS-AAm copolymers with different amounts of crosslinker and their swelling behavior in distilled water. In Fig. 3b, an increase in the $n_{T/nMBAA}$ ratio of the synthesized hydrogels from 25 to 2000 resulted in an increase in the equilibrium swelling value from 16.38 to 1510.39 g H_2O/g gel. In the polymerization reaction, different amounts of crosslinker ($n_{T/nMBAA}$ ratios of 25–2000) were used by taking 0.065 mol of AAm and 0.010 mol of SVS. Different amounts of crosslinking agent ($n_{T/nMBAA}$: 25–2000 ratios) were used with AAm amount of 0.060 mol and SVS amount of 0.015 mol to synthesize SVS-AAm copolymers. The swelling equilibrium values of the obtained hydrogels over time in distilled water were shown and the swelling equilibrium values were given in Fig. 3c. When the $n_{T/nMBAA}$ ratio of the synthesized hydrogels increased from 25 to 2000, the swelling equilibrium value increased from 15.53 to 1341.54 g H_2O/g gel. As seen in Fig. 3d, it was observed that the equilibrium swelling value of the synthesized hydrogels increased from 16.35 to 2063.61 g H_2O/g gel. According to the experimental results (Fig. 3e), the equilibrium swelling value of the synthesized hydrogels increased from 11.84 to 866.92 g H_2O/g gel value. Similarly, as seen in Fig. 3f, the equilibrium swelling value of the synthesized hydrogels increased from 17.42 to 312.18 g H_2O/g gel value. Additionally, as observed from Fig. 3g, the equilibrium swelling value of the synthesized hydrogels increased from 14.45 to 81.47 g H_2O/g gel value as the $n_{T/nMBAA}$ ratio of the hydrogels increased from 25 to 100. The results shown in Figs. 3a–g indicates that there was a noticeable decrease in the equilibrium swelling values as the amount of crosslinker increased while maintaining the monomer concentration constant. This is due to the fact that a higher density of crosslinks inside the gel is generated by a higher crosslinker concentration, which in turn reduces the distances between copolymer chain gaps. Because of this, the network structure cannot expand as easily, which makes it difficult for water to enter and decreases the amount of water that the gels can absorb. This phenomenon can be explained through the fact that a higher crosslinker concentration results in a more tightly bonded polymer network with a smaller size, which restricts the diffusion of water molecules into the polymer gel matrix [42, 43].

In Fig. 4**,** swelling behavior of multi-network SVS-AAm-MBAA hydrogel with different SVS compositions (n_T/n_{MBAA}): (a) n_{MBAA}: 3×10^{-3} mol, (b) n_{MBAA}: 1.5×10^{-3} mol, (c) n_{MBAA}: 7.5×10^{-4} mol, (d) $n_{MBAA}=3\times10^{-4}$ mol, (e) $n_{MBAA}=7.5\times10^{-5}$ mol, (f) n_{MBAA}: 3.75×10^{-5} mol and n_T: 0.075 mol, respectively (T: SVS + AAm) was presented.

As seen in Fig. 4, the equilibrium swelling values of the synthesized gels increased from 44.71 to 2063.60 g H_2O/g gel in distilled water with the increase of n_{SVS}/n_{AAm} ratio, which corresponds to the increase in the amount of SVS in the gel. When the n_{SVS}/n_{AAm} ratio was 0.087, the pure water equilibrium swelling value of the gel was 1510.39 g H_2O/g gel, and when this ratio increased to 0.154, which means an increase in the SVS content in the gel, the swelling equilibrium value of the gel was observed to be 1341.54 g H_2O/g gel. Upon examining Fig. 4a–e, it was observed that while the amount of SVS increased, there was a decrease or no significant change in the swelling values and equilibrium swelling values of the gels synthesized using a high amount of crosslinker. The reason for the decrease in swelling values or lack of significant change is interpreted as the irregular network structure of the crosslinked polymers synthesized using a high amount of crosslinker. When examining experimental results, it can be seen that as the amount of SVS in the hydrogel increased, the equilibrium swelling values also increased. This can be explained by the increase in the number of ionic groups in the gel, which increases the interchain expansion and results in higher swelling values for the multi-network SVS-AAm-MBAA hydrogel.

Swelling Kinetic Models of the Multi-Network SVS-AAm-MBAA Hydrogel

Figures 5 and 6 provide information regarding the swelling kinetic models of SVS-AAm-MBAA hydrogel, which is composed of multiple networks. The graph exhibits the changes in hydrogel swelling over time, which are influenced by the concentration of MBAA and the ratio of SVS/AAm to crosslinker (MBAA). Different lines on the graph correspond to various combinations of these factors. By examining the data presented in Figs. 5, 6, we can gain a better understanding of how changes in the key parameters, namely monomer/crosslinker ratios (AAm-MBAA: 25–2000) and MBAA concentrations (3×10^{-3} mol–3.75×10^{-5} mol), affect the swelling kinetics of the multi-network SVS-AAm-MBAA hydrogel. In Fig. 5, the Voigt model graphs of SVS-AAm-MBAA hydrogel at various AAm-MBAA ratios at 25, 50, 100, 250, 1000, 1500, and 2000. In Fig. 6**,** Voigt model graphs of SVS-AAm-MBAA hydrogel with varying SVS-AAm ratios: 0.087, 0.154, 0.250, 0.500, 0.875, and 1.143.

In Tables 2, 3, Voigt model parameters of hydrogels containing different amounts of cross-linker and SVS were given, respectively.

The findings from Tables 2, 3, obtained through calculations using the Voigt kinetic model parameters, have provided ineresting insights into the behavior of the

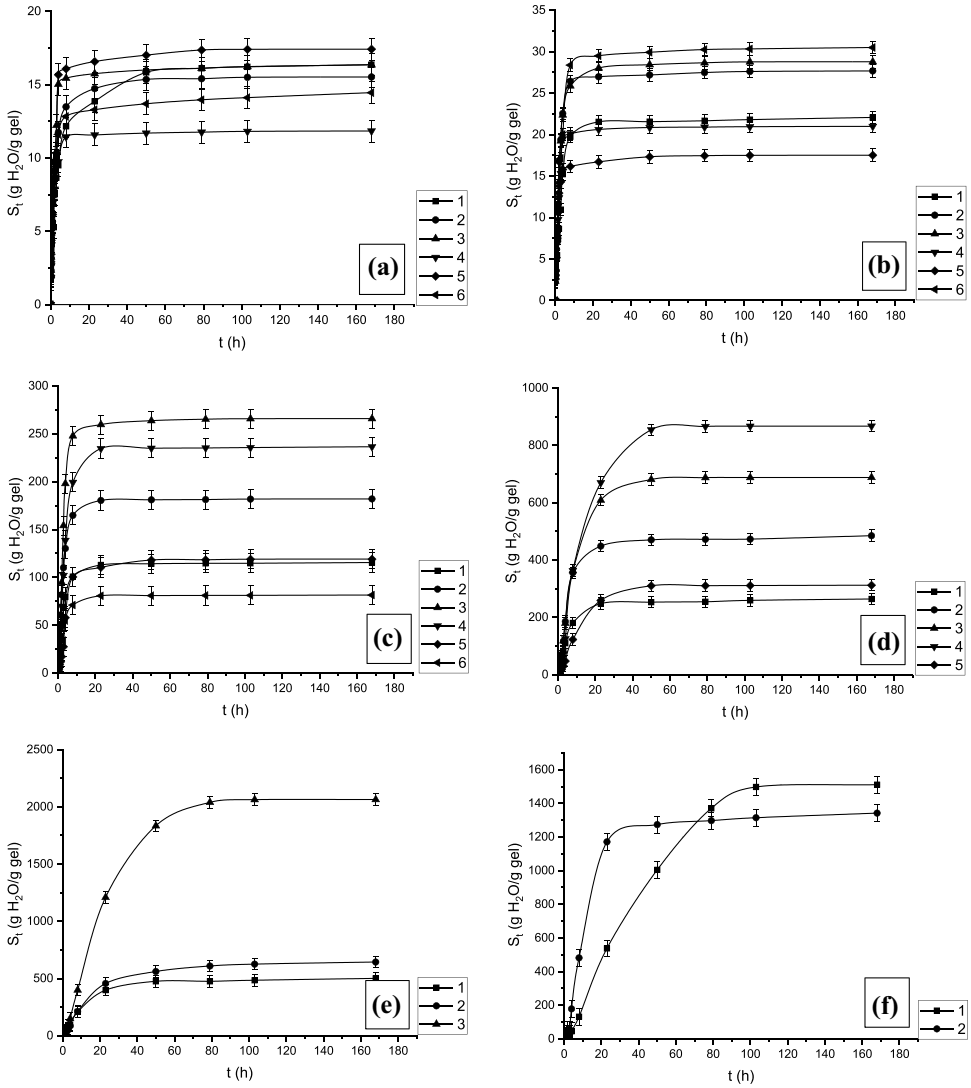

Fig. 4 Swelling behavior of multi-network SVS-AAm-MBAA hydrogel with different SVS compositions (n_T/n_{MBAA}): **a** n_{MBAA}: 3×10^{-3} mol, **b** n_{MBAA}: 1.5×10^{-3} mol, **c** n_{MBAA}: 7.5×10^{-4} mol, **d** $n_{MBAA}=3\times10^{-4}$ mol, **e** $n_{MBAA}=7.5\times10^{-5}$ mol, **f** n_{MBAA}: 3.75×10^{-5} mol and n_T: 0.075 mol

SVS-AAm-MBAA hydrogel. The data clearly demonstrate that the hydrogel exhibited varying τ values depending on the AAm-MBAA and SVS ratios. Moreover, a distinct correlation emerged between these ratios and the swelling rate of the hydrogel. Specifically, an increase in both the AAm-MBAA and SVS ratios resulted in a gradual reduction in the hydrogel's swelling rate. In simpler terms, higher AAm-MBAA and SVS ratios were associated with a slower rate of swelling. These findings significantly enhance our understanding of the intricate relationship between the AAm-MBAA and SVS ratios and their impact on the hydrogel's swelling behavior, as elucidated by the Voigt kinetic model.

Removal of Paracetamol by Multi-Network SVS-AAm-MBAA Hydrogel

To investigate the effect of prepared hydrogels on the removal of paracetamol from an aqueous solution, varying amounts of copolymer (ranging from 0.02 to 0.15 g) were used in the experiment. To ensure the accuracy and reliability of the results, various factors that could affect the outcome of the experiment, such as the volume of the solution (10 mL), the concentration of paracetamol in the solution (20 ppm), temperature (293 K), and agitation time (60 min.) were controlled. By changing the amount of copolymer and keeping the other factors constant, the capacity of the hydrogel to remove paracetamol from the solution was evaluated by calculating kinetic model parameters, isotherm constants, and thermodynamic parameters. The experimental methodology used in this study was thorough and systematic, providing valuable insights into the performance of hydrogels with different copolymer amounts for the removal of paracetamol. To determine the most effective copolymer composition for the hydrogel, various hydrogels were prepared with different amounts of n_{MBAA}, n_{AAm}, and n_{SVS}/n_{AAm}. The hydrogel with the highest swelling potential was chosen for the adsorption study, which involved weighing the dry

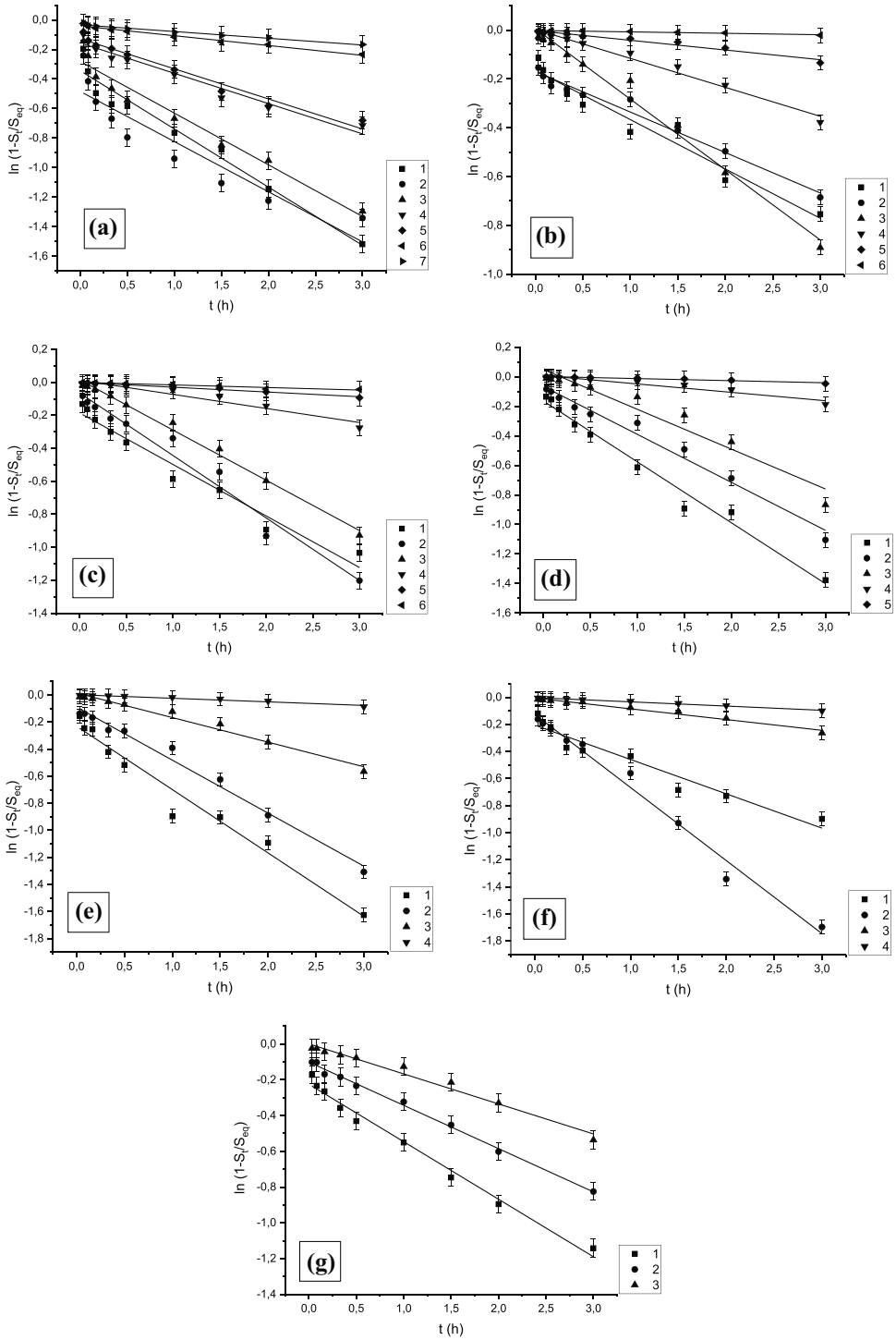

Fig. 5 Voigt model graphs of SVS-AAm-MBAA hydrogel with varying AAm+SVS-MBAA ratios: 25(1), 50(2), 100(3), 250(4), 1000(5), 2000(6), and 1500(7). Black square (1), black circle (2), black triangle (3), black down-pointing triangle (4), black diamond suit (5), black left-pointing triangle (6), black right-pointing triangle (7)

gel at varying adsorbent amounts and measuring the % adsorption values of the adsorbents after being exposed to a 20 ppm paracetamol solution for 1 h in a shaker. The spectrophotometric measurement of the filtrate before and after absorption at a wavelength of 243 nm enabled accurate determination of the absorption values. The results were presented in Fig. 7, which clearly shows the effect of changing the adsorbent dose on the % adsorption values.

The results in Fig. 7a demonstrate that increasing the amount of adsorbent leads to an increase in % adsorption values until equilibrium is reached at 0.05 g of adsorbent. Thus, future studies investigating the effects of temperature, time, and paracetamol concentration should use 0.05 g of adsorbent. Figure 7b illustrates the adsorption performance of the prepared hydrogel at different drug concentrations ranging from 0.0331 mmol/L

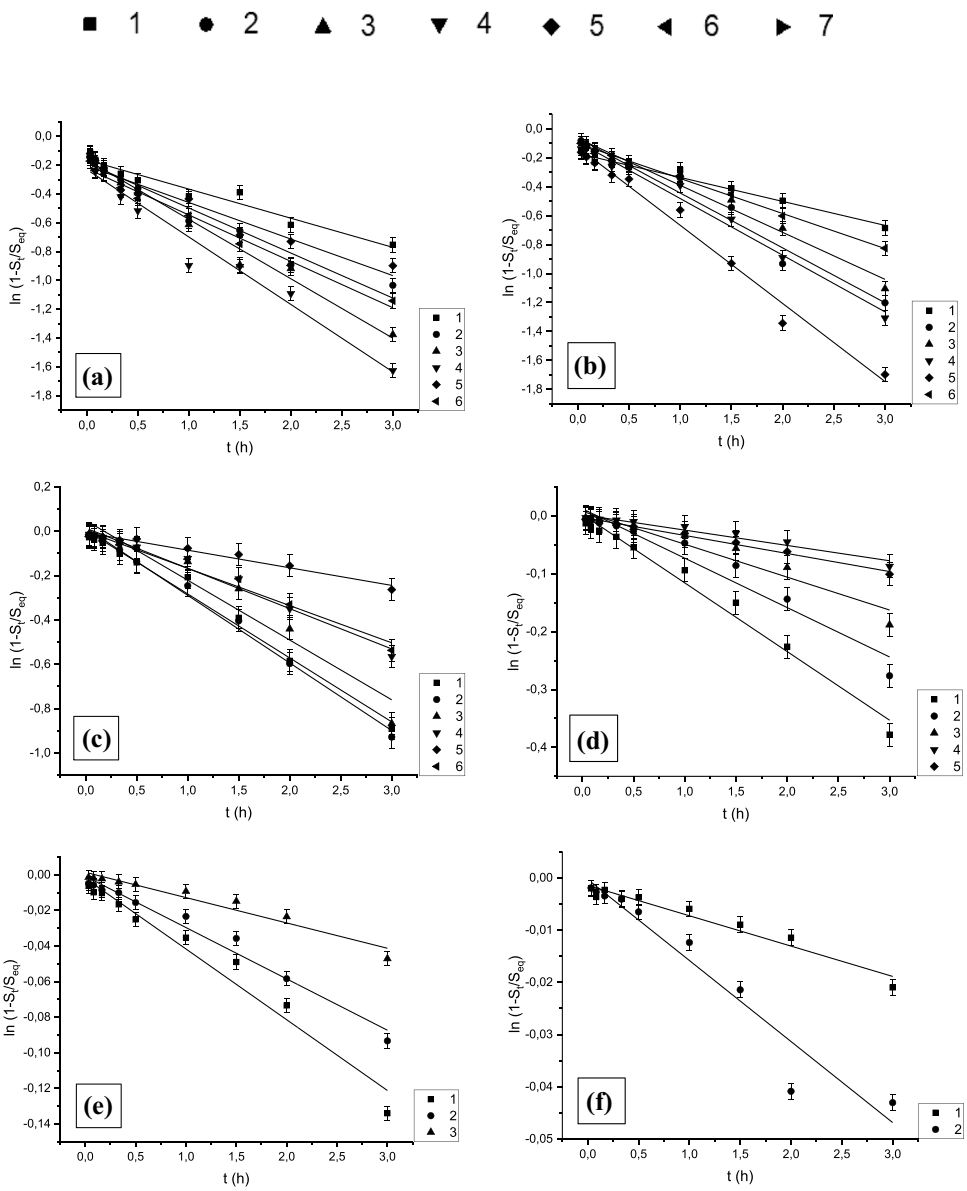

Fig. 6 Voigt model graphs of SVS-AAm-MBAA hydrogel with varying SVS-AAm ratios: 0.087(1), 0.154(2), 0.250(3), 0.500(4), 0.875(5) and 1.143(6). Black square (1), black circle (2), black triangle (3), black down-pointing triangle (4), black diamond suit (5), black left-pointing triangle (6)

to 0.1984 mmol/L. The % adsorption value increased by 25.79% and 51.04% respectively, indicating a higher adsorption capacity at higher drug concentrations. A mathematical model known the Freundlich isotherm is used to explain how solutes adsorb to the surfaces of adsorbents. The experimental results showed that the adsorption process followed the Freundlich isotherm model, with a K_F value of 1.248 mmol/g and an "n" value of 1.757 indicating successful adsorption (Fig. 7c). However, plotting the C_e/q_e values against C_e in Fig. 7d did not result in a linear relationship, indicating that the values obtained using the hydrogel as an adsorbent and varying paracetamol concentrations did not fit the Langmuir isotherm. In Table 4**,** the calculated results of parameters of isotherm, kinetic and thermodynamic equations for the adsorption paracetamol on hydrogel from aqueous solutions were given.

The adsorption energy for paracetamol adsorption onto the hydrogel at 30 °C was found to be 6 kJ/mol, indicating an active adsorption mechanism that is close to the chemical adsorption value of 8 kJ/mol (Fig. 7e). Based on these observations, it can be concluded that the adsorption process is primarily a chemical adsorption. The graph in Fig. 7f shows that as the duration of paracetamol adsorption onto the hydrogel increases, the adsorption rate initially increases rapidly. Subsequently, the rate of increase slows down in the second stage, and equilibrium values are reached within 30–60 min. The adsorption value at 60 min is considered as the equilibrium adsorption value. We evaluated the experimental results and applied the modified Freundlich kinetic model. The kinetic equation constants were calculated as a: 9.11×10^{-3} and b: 0.0968 (Fig. 7g). However, the low correlation coefficient was

Table 2 Voigt model parameters of hydrogels containing different amounts of cross-linker

$n_{AAm+SVS}/n_{MBAA}$	τ(h)	R^2
n_{AAm}: 0.075 mol and n_{SVS}: 0 mol		
25	2.54	0.964
50	2.95	0.861
100	2.86	0.957
250	4.88	0.961
1000	15.06	0.982
1500	26.04	0.979
2000	21.93	0.981
n_{AAm}: 0.069 mol, n_{SVS}: 0.006 mol, n_T: 0.075 mol, and n_{SVS}/n_{AAm}: 0.087		
25	4.95	0.952
50	6.03	0.979
100	3.47	0.987
250	8.43	0.982
1000	25.13	0.966
2000	172.41	0.953
n_{AAm}: 0.065 mol, n_{SVS}: 0.010 mol, n_T: 0.075 mol, and n_{SVS}/n_{AAm}: 0.154		
25	3.20	0.965
50	2.64	0.974
100	3.28	0.994
250	1.17	0.947
1000	33.46	0.977
2000	64.52	0.940
$n_{SVS+AAm}/n_{MBAA}$	τ(h)	R^2
n_{AAm}: 0.060 mol, n_{SVS}: 0.015 mol, n_T: 0.075 mol, and n_{svs}/n_{AAm}: 0.250		
25	2.43	0.984
50	3.08	0.981
100	3.75	0.944
250	17.61	0.938
1000	70.42	0.946
n_{AAm}: 0.050 mol, n_{SVS}: 0.025 mol, n_T: 0.075 mol, and n_{svs}/n_{AAm}: 0.500		
25	2.14	0.968
50	2.55	0.987
100	5.50	0.979
250	37.74	0.966
n_{AAm}: 0.040 mol, n_{SVS}: 0.035 mol, n_T: 0.075 mol, and n_{svs}/n_{AAm}: 0.875		
25	3.94	0.935
50	1.85	0.986
100	12.59	0.977
250	32.05	0.992
n_{AAm}: 0.035 mol, n_{SVS}: 0.040 mol, n_T: 0.075 mol, and n_{svs}/n_{AAm}: 1.143		
25	3.11	0.987
50	4.13	0.996
100	5.95	0.979

observed, indicating that the model did not fit well with the experimental data. Later, we tried to fit the modified Freundlich kinetic model obtained over time, and found that R^2 was 0.945, which is a relatively high value indicating a good fit between the model and the experimental data over time. According to results (Fig. 7h), the hydrogel's initial adsorption rate was determined to be $A = 8.1 \times 10^6$, and the adsorption constant was found

Table 3 Voigt model parameters of hydrogels containing different amounts of SVS

n_{SVS}/n_{AAm}	τ(h)	R^2
n_{MBAA}: 3×10^{-3} mol and n_T: 0.075 mol		
0.087	4.95	0.952
0.154	3.20	0.965
0.250	2.43	0.984
0.500	2.14	0.968
0.875	3.94	0.935
1.143	3.11	0.987
n_{MBAA}: 1.5×10^{-3} mol and n_T: 0.075 mol		
0.087	6.03	0.979
0.154	2.64	0.974
0.250	3.08	0.981
0.500	1.85	0.981
0.875	2.55	0.986
1.143	4.13	0.987
n_{MBAA}: 7.5×10^{-4} mol and n_T: 0.075 mol		
0.087	3.47	0.986
0.154	3.28	0.994
0.250	3.71	0.944
0.500	5.50	0.979
0.875	12.59	0.977
1.143	15.95	0.979
$n_{SVS+AAm}/n_{MBAA}$	τ(h)	R^2
n_{MBAA}: 3×10^{-4} mol and n_T: 0.075 mol		
0.087	8.43	0.982
0.154	11.72	0.947
0.250	17.61	0.938
0.500	37.74	0.957
0.875	32.05	0.992
n_{MBAA}: 7.5×10^{-5} mol and n_T: 0.075 mol		
0.087	25.13	0.966
0.154	34.60	0.977
0.250	70.42	0.946
n_{MBAA}: 3.75×10^{-5} mol and n_T: 0.075 mol		
0.087	172.41	0.952
0.154	64.52	0.940

to have the value $B = 1 \times 10^{-3}$. The resulting correlation coefficient values, however, were found to be poor when the adsorption data obtained through time was fitted to the Elovich kinetic model. The equilibrium initial adsorption rate increased with an increase in the initial paracetamol concentration, according to the analysis of the effect of the starting paracetamol concentration on the adsorption process. This implies that the hydrogel can absorb paracetamol at higher starting concentrations with greater efficiency. The rate at which paracetamol is absorbed onto the hydrogel is represented by the adsorption rate constant, which decreases with increasing starting concentration. This decline suggests the possibility that the hydrogel's ability to adsorb substances at greater concentrations may have been constrained or saturated, which would explain the decreased rate of adsorption. In order to maximize the adsorption process, a balance must be found between the initial paracetamol concentration and the hydrogel's capacity for adsorption. As a result, when the paracetamol adsorption data obtained over time on hydrogel were applied to the pseudo-first-order kinetic rate model, the rate constant was found to be $k = 0.224$ L/min and the amount of paracetamol adsorbed onto the hydrogel was $q_e = 3.69 \times 10^{-3}$ mmol/g. However,

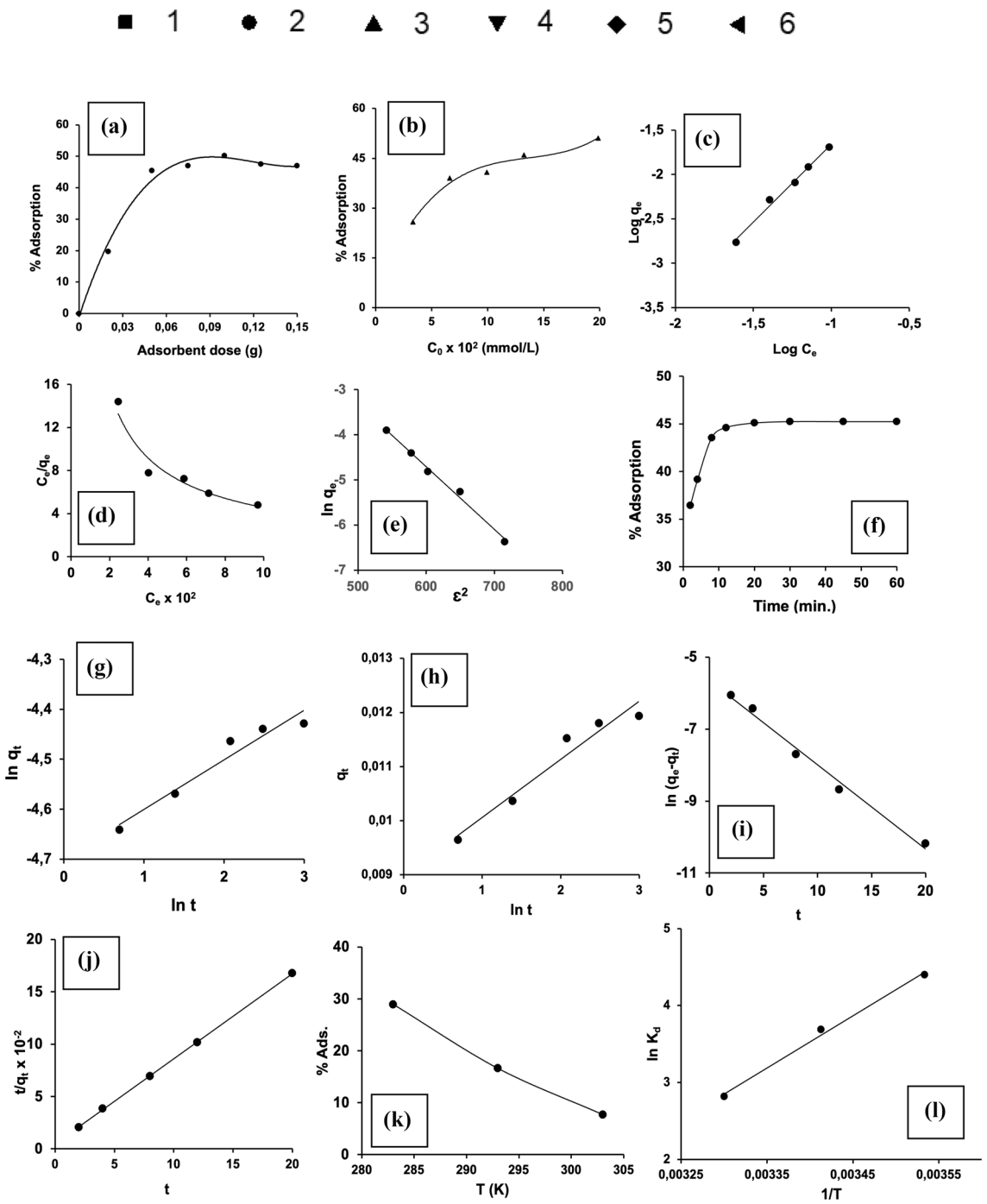

Fig. 7 The effect of **a** adsorbent dose, **b** drug concentration, Isotherms **c** Freundlich, **d** Langmuir, **e** D-R, **f** the effect of contac time, **g** modified Freundlich, Kinetic model **h** Elovich, **i** pseudo-first-order, **j** pseudo-second-order, **k** effect of temperature, **l** 1/T-ln Kd graph

when the time-dependent adsorption data was applied to the pseudo-first-order kinetic model, a very good correlation coefficient ($R^2 = 0.989$) value was not obtained (in Fig. 7i). The t/qt graph drawn against time in the application of the adsorption data to the pseudo-second-order kinetic model is given in Fig. 7j. The adsorption rate constant obtained from the slope and intercept values of the graph was k = 129.81 g/mmol min and the equilibrium adsorption capacity value was $q_e = 1.23 \times 10^{-2}$ mmol/g. Upon examination of the results, it can be observed that the correlation coefficient obtained by applying the time-dependent adsorption data to the pseudo-second-order kinetic model is quite high ($R^2 = 0.999$). Therefore, it can be said that the adsorption kinetics fits much better

Table 4 The calculated results of parameters of isotherm, kinetic and thermodynamic equations for the adsorption paracetamol on hydrogel from aqueous solutions

Freundlich Isotherm $\log q_e = \log K_f + n \log C_e$	C_0 (mmg/L)		K_F (mmol/g)	n		R^2
	5, 10, 15, 20, 30		1.248	1.757		0.990
Duninin Radushkevich (D-R) Isotherm $\ln q_e = \ln q_m - K\varepsilon^2$	C_0 (mmg/L)		q_m (mmol/g)	$E = (-2K)^{1/2}$ (kJ/mol)		R^2
	5, 10, 15, 20, and 30		38.59	6		0.992
Modified Freundlich kinetic equation $\ln q_t = \ln a + b \ln t$	C_0 (mmg/L)		a	b		R^2
	20		9.11×10^{-3}	0.0968		0.945
Elovich kinetic equation $q_t = (1/B) \ln (AB) + (1/B) \ln t$	C_0 (mmg/L)		A	B		R^2
	20		8.10×10^{6}	1×10^{3}		0.950
Pseudo-first order kinetic equation	C_0 (mmg/L)		q_e (mmol/g)	k_1 (min^{-1})		R^2
$\ln(q_e - q_t) = \ln q_e - kt$	20		0.224	3.69×10^{-3}		0.989
Pseudo-second order kinetics equation $t/q_t = 1/kq_e^2 + (1/q_e)\, t$	C_0 (mmg/L)		q_e (mmol/g)	k_2 (g/mmol min)		R^2
	20		1.23×10^{-2}	129.81		0.999
Thermodynamic parameters $\ln K_D = \Delta S^0/R - \Delta H^0/RT$, $\Delta \mathbf{G}^0 = \Delta \mathbf{H}^0 - T\, \Delta \mathbf{S}^0$	C_0 (mmg/L)	ΔH° (kJ/mol)	ΔS° (kJ/mol K)	$\Delta G°_{283}$ (kJ/mol)	$\Delta G°_{293}$ (kJ/mol)	$\Delta G°_{303}$ (kJ/mol)
	20	− 56.37	− 0.162	− 103.9	− 105.6	107.2

to the pseudo-second-order kinetic model than to other models. Thermodynamic parameters related to paracetamol adsorption onto hydrogel was given. The temperature dependence of paracetamol adsorption onto the copolymer was examined to calculate the thermodynamic parameters of adsorption. ΔH°, ΔG°, and ΔS° values were calculated. The ΔH° value was found to be − 56.37 kJ/mol, the ΔS° value was − 0.162 kJ/mol K, and the ΔG° values were calculated as − 103.9 kJ/mol at 283 K, − 105.6 kJ/mol at 293 K, and − 107.2 kJ/mol at 303 K. As the ΔH° value of the reaction is negative, it is an exothermic reaction. When the data is examined, the reaction takes place spontaneously at values where ΔG° and ΔS° are less than zero.

In literature Safarzadeh et al. reported the adsorption ability evaluation of the poly(methacrylic acid-co-acrylamide)/cloisite 30B nanocomposite hydrogel as a new adsorbent for cationic methylene blue (MB) dye removal [44]. In another study, Zhao et al. developed novel acrylamide/acrylic acid cellulose hydrogels for the adsorption of heavy metal ions (Cu (II), Pb (II) and Cd (II) ions) [45]. Dave et al. investigated metformin hydrochloride drug removal performance of the gum ghatti-cl-poly(N-isopropyl acrylamide-co-acrylic acid)/CoFe2O4 nanocomposite hydrogel [46]. In the research papers reported in the literature, the adsorption capacity of various hydrogels for different pollutants was investigated. Our investigation of a copolymer's adsorption behavior for removing paracetamol, a widely used pharmaceutical substance, from aqueous solutions, however, is novel in this study. Our research offers crucial light on the thermodynamics of paracetamol adsorption onto the produced hydrogel, which showed a high capacity for paracetamol adsorption.

The redox reaction between MSA and Ce(IV) dissolved in a sulfuric acid solution leads to the formation of radicals through one-electron transfer. The radical formation reaction between MSA and Ce(IV) in an acid-aqueous medium was previously described in studies [47, 48]. The chemical mechanisms for the formation in the crosslinking copolymerization of SVS-AAm-MBAA are shown in Fig. 8.

The multi-network SVS-AAm-MBAA hydrogel has the potential to create effective adsorbent materials for pharmaceutical uses, particularly removing paracetamol from contaminated water sources. However, as with any new material, there are potential limitations that need to be addressed before it can be widely used in practical applications. In addition to the long-term durability and stability

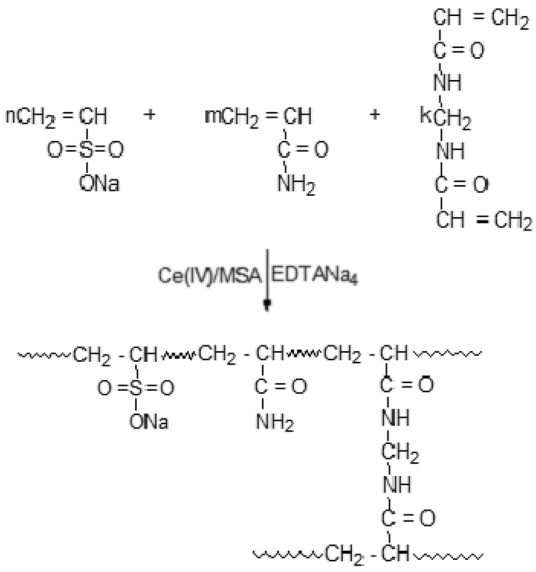

Fig. 8 Product formation mechanism of SVS-AAm- MBAA hydrogel

of the hydrogel under different environmental conditions, it is important to consider any potential negative impacts on water quality. Despite these limitations, this study provides important insights into the potential of the SVS-AAm-MBAA hydrogel as an efficient adsorbent for pharmaceutical chemicals. By acknowledging and addressing potential drawbacks, we can work towards optimizing the use of hydrogels in water treatment and creating environmentally sustainable water filtration techniques. Overall, this study contributes to our understanding of creating efficient and sustainable water treatment methods, which is crucial for addressing the global challenge of water pollution.

Conclusion

In conclusion, we showed that the multi-network SVS-AAm-MBAA hydrogel was successfully synthesized employing the Ce(IV)-MSA initiator system, leading to an increase in water absorption capacity. The experiment also showed that lowering the cross-linker concentration increased the swelling equilibrium values in AAm hydrogels begun using Ce(IV) sulfate-mercaptosuccinic acid without SVS. Additionally, the hydrophilic groups on SVS caused an increase in swelling values following its addition to the copolymeric system up to a point. SEM analysis evaluated the surface morphology of the pure AAm/SVS/MBAA hydrogel and paracetamol-loaded AAm/SVS/MBAA hydrogel, confirming their structural homogeneity and partial smoothness. Significant changes in surface properties were observed due to paracetamol adsorption, with noticeable differences in surface roughness between the drug-loaded and pure hydrogels. These findings suggest an interaction between the drug molecules and the hydrogel matrix, potentially leading to surface adsorption. The study demonstrates the synthetic copolymer's potential as an efficient adsorbent for removing paracetamol from aqueous solutions, suggesting possibilities for water treatment. However, several factors, including raw material accessibility, synthesis approach, and contaminant removal effectiveness need to be considered to establish the viability of producing hydrogels on a wide scale for water treatment. All these factors can be considered in future study, which will then perform a cost–benefit analysis to determine whether making hydrogels for water treatment is economically feasible. This study highlights the potential of high-performance copolymers to address environmental issues including water pollution and advances the development of these materials for a variety of materials science applications.

Author Contributions SMS: Conceptualization, formal analysis, investigation, RT: formal analysis, CÖ: Writing—review and editing, supervision and SK: Writing—review and editing, data curation, visualization.

Funding This paper did not receive any funding.

Declarations

Conflict of interest All authors confirm that there are no known conflicts of interest associated with this publication.

Ethical Approval Not applicable.

References

1. Tan J, Luo Y, Guo Y et al (2023) Development of alginate-based hydrogels: crosslinking strategies and biomedical applications. Int J Biol Macromol 239:124275. https://doi.org/10.1016/J.IJBIOMAC.2023.124275
2. Ghobadifar V, Marandi GB, Kurdtabar M, Bardajee GR (2023) Removal of Pb(II) and Cd(II) by MnFe2O4@SiO2@VTMS nanocomposite hydrogel from aqueous solutions. J Polym Environ. https://doi.org/10.1007/S10924-022-02670-4/TABLES/7
3. Özkahraman B, Özbaş Z (2020) Removal of Al(III) ions using gellan gum-acrylic acid double network hydrogel. J Polym Environ 28:689–698. https://doi.org/10.1007/S10924-019-01636-3/FIGURES/9
4. Tian B, Liu J (2023) Smart stimuli-responsive chitosan hydrogel for drug delivery: a review. Int J Biol Macromol 235:123902. https://doi.org/10.1016/J.IJBIOMAC.2023.123902
5. Yuan N, Shao K, Huang S, Chen C (2023) Chitosan, alginate, hyaluronic acid and other novel multifunctional hydrogel dressings for wound healing: a review. Int J Biol Macromol 240:124321. https://doi.org/10.1016/J.IJBIOMAC.2023.124321
6. Chen Q, He Y, Li Q et al (2023) Intelligent design and medical applications of antimicrobial hydrogels. Colloid Interface Sci Commun 53:100696. https://doi.org/10.1016/J.COLCOM.2023.100696
7. Li H, Wu C, Yu X, Zhang W (2023) Recent advances of PVA-based hydrogels in cartilage repair application. J Market Res 24:2279–2298. https://doi.org/10.1016/J.JMRT.2023.03.130
8. Ren J, Wang X, Zhao L et al (2022) Double network gelatin/chitosan hydrogel effective removal of dyes from aqueous solutions. J Polym Environ 30:2007–2021. https://doi.org/10.1007/S10924-021-02327-8/TABLES/6
9. Alesaeidi S, Kahrizi MS, Ghorbani Tajani A et al (2023) Soy protein isolate/sodium alginate hybrid hydrogel embedded with hydroxyapatite for tissue engineering. J Polym Environ 31:396–405. https://doi.org/10.1007/S10924-022-02635-7/FIGURES/9
10. Rafati Z, Sirousazar M, Hassan ZM, Kheiri F (2020) Honey-loaded egg white/poly(vinyl alcohol)/clay bionanocomposite hydrogel wound dressings. In vitro and in vivo evaluations. J Polym Environ 28:32–46. https://doi.org/10.1007/S10924-019-01586-W/FIGURES/13
11. Nguyen CT, Vu MQ, Phan TT et al (2020) Novel pH-sensitive hydrogel beads based on carrageenan and fish scale collagen for allopurinol drug delivery. J Polym Environ 28:1795–1810. https://doi.org/10.1007/S10924-020-01727-6/TABLES/9
12. Jiang M, Simayi R, Sawut A et al (2023) Modified β-cyclodextrin hydrogel for selective adsorption and desorption for cationic dyes. Colloids Surf A Physicochem Eng Asp 661:130912. https://doi.org/10.1016/J.COLSURFA.2022.130912

13. Zhu H, Chen S, Luo Y (2023) Adsorption mechanisms of hydrogels for heavy metal and organic dyes removal: a short review. J Agric Food Res 12:100552. https://doi.org/10.1016/J.JAFR.2023.100552
14. Zhang R, Liu B, Ma J, Zhu R (2022) Preparation and characterization of carboxymethyl cellulose/chitosan/alginic acid hydrogels with adjustable pore structure for adsorption of heavy metal ions. Eur Polym J 179:111577. https://doi.org/10.1016/J.EURPOLYMJ.2022.111577
15. Bardajee GR, Mahmoodian H, Boraghi SA et al (2023) Nanoporous hydrogel absorbent based on salep: swelling behavior and methyl orange adsorption capacity. Environ Res 225:115571. https://doi.org/10.1016/J.ENVRES.2023.115571
16. Zhu H, Chen S, Duan H et al (2023) Removal of anionic and cationic dyes using porous chitosan/carboxymethyl cellulose-PEG hydrogels: optimization, adsorption kinetics, isotherm and thermodynamics studies. Int J Biol Macromol 231:123213. https://doi.org/10.1016/J.IJBIOMAC.2023.123213
17. Yu X, Li X, Kan L et al (2023) Double network microcrystalline cellulose hydrogels with high mechanical strength and biocompatibility for cartilage tissue engineering scaffold. Int J Biol Macromol 238:124113. https://doi.org/10.1016/J.IJBIOMAC.2023.124113
18. Yang R, Wang R, Abbaspoor S et al (2023) In vitro and in vivo evaluation of hydrogel-based scaffold for bone tissue engineering application. Arab J Chem 16:104799. https://doi.org/10.1016/J.ARABJC.2023.104799
19. Song JE, Lim S, Kim DH, Cho EC (2016) Controlling molecular orientations of hydrogels in oil–drug@hydrogel particle delivery systems for pH-selective/sustained release and stabilization of bioactive drugs. Colloids Surf A Physicochem Eng Asp 490:49–58. https://doi.org/10.1016/J.COLSURFA.2015.11.032
20. Davidson-Rozenfeld G, Stricker L, Simke J et al (2019) Light-responsive arylazopyrazole-based hydrogels: their applications as shape-memory materials, self-healing matrices and controlled drug release systems. Polym Chem 10:4106–4115. https://doi.org/10.1039/C9PY00559E
21. Wang W, Ummartyotin S, Narain R (2023) Advances and challenges on hydrogels for wound dressing. Curr Opin Biomed Eng 26:100443. https://doi.org/10.1016/J.COBME.2022.100443
22. Kim Y, Jeong D, Shinde VV et al (2020) Azobenzene-grafted carboxymethyl cellulose hydrogels with photo-switchable, reduction-responsive and self-healing properties for a controlled drug release system. Int J Biol Macromol 163:824–832. https://doi.org/10.1016/J.IJBIOMAC.2020.07.071
23. Zheng S, Cohen N, Liu Z (2022) Large deformation adhesion study of polymetric hydrogel under different stimuli. Mech Mater 165:104174. https://doi.org/10.1016/J.MECHMAT.2021.104174
24. Zhang N, Zheng S, Liu Z (2017) Numerical simulation and experimental study of crack propagation of polydimethylsiloxane. Procedia Eng 214:59–68. https://doi.org/10.1016/J.PROENG.2017.08.191
25. Zheng Y, Wang J, Ye H et al (2020) A mixed isogeometric analysis approach for the transient swelling of hydrogel. Comput Methods Appl Mech Eng 372:113384. https://doi.org/10.1016/J.CMA.2020.113384
26. Zheng S, Huang R, Lin R, Liu Z (2022) A phase field solution for modelling hyperelastic material and hydrogel fracture in ABAQUS. Eng Fract Mech 276:108894. https://doi.org/10.1016/J.ENGFRACMECH.2022.108894
27. Jiang K, Zhou X, He T (2022) The synthesis of bacterial cellulose-chitosan zwitterionic hydrogels with pH responsiveness for drug release mechanism of the naproxen. Int J Biol Macromol 209:814–824. https://doi.org/10.1016/J.IJBIOMAC.2022.03.216
28. Zheng S, You H, Li H, Lam KY (2023) A model for fracture of temperature-sensitive hydrogel with diffusion and large deformation. Eng Fract Mech 281:109138. https://doi.org/10.1016/J.ENGFRACMECH.2023.109138
29. Zhang G, Guo TF, Zhou Z et al (2019) A phase-field model for fracture in water-containing soft solids. Eng Fract Mech 212:180–196. https://doi.org/10.1016/J.ENGFRACMECH.2019.02.035
30. Mir A, Kumar A, Riaz U (2023) Synthesis and characterization of conducting polymer/alginate composite hydrogels: effect of conducting polymer loading on the release behaviour of metformin drug. J Mol Liq 372:121193. https://doi.org/10.1016/J.MOLLIQ.2022.121193
31. Kambayashi A, Dressman JB (2019) A novel in vivo predictive dissolution testing coupled with a modeling and simulation for hydrogel matrix monolithic extended release oral dosage forms. Eur J Pharm Sci 138:105044. https://doi.org/10.1016/J.EJPS.2019.105044
32. Das D, Das R, Ghosh P et al (2013) Dextrin cross linked with poly(HEMA): a novel hydrogel for colon specific delivery of ornidazole. RSC Adv 3:25340–25350. https://doi.org/10.1039/C3RA44716B
33. Rahmani P, Shojaei A (2022) Developing tough terpolymer hydrogel with outstanding swelling ability by hydrophobic association cross-linking. Polymer (Guildf) 254:125037. https://doi.org/10.1016/J.POLYMER.2022.125037
34. Zahedinejad M, Sohrabi N, Mohammadi R (2023) Magnetic multi-walled carbon nanotubes as an efficient sorbent for pirimicarb removal from aqueous solutions in continuous (FBAC) and batch formats: thermodynamic, kinetic, isotherm study, optimization and modeling by RSM-ANN. J Mol Liq 370:120915. https://doi.org/10.1016/J.MOLLIQ.2022.120915
35. Jayakumar V, Govindaradjane S, Rajasimman M (2021) Efficient adsorptive removal of Zinc by green marine macro alga *Caulerpa scalpelliformis*—characterization, optimization, modeling, isotherm, kinetic, thermodynamic, desorption and regeneration studies. Surf Interfaces 22:100798. https://doi.org/10.1016/J.SURFIN.2020.100798
36. Karaman C, Karaman O, Show PL et al (2022) Congo red dye removal from aqueous environment by cationic surfactant modified-biomass derived carbon: equilibrium, kinetic, and thermodynamic modeling, and forecasting via artificial neural network approach. Chemosphere 290:133346. https://doi.org/10.1016/J.CHEMOSPHERE.2021.133346
37. Varank G, Demir A, Yetilmezsoy K et al (2012) Removal of 4-nitrophenol from aqueous solution by natural low-cost adsorbents. Indian J Chem Technol 19:7–25
38. Pandiarajan A, Kamaraj R, Vasudevan S, Vasudevan S (2018) OPAC (orange peel activated carbon) derived from waste orange peel for the adsorption of chlorophenoxyacetic acid herbicides from water: adsorption isotherm, kinetic modelling and thermodynamic studies. Bioresour Technol 261:329–341. https://doi.org/10.1016/J.BIORTECH.2018.04.005
39. Saber-Samandari S, Gazi M (2015) Pullulan based porous semi-IPN hydrogel: synthesis, characterization and its application in the removal of mercury from aqueous solution. J Taiwan Inst Chem Eng 51:143–151. https://doi.org/10.1016/J.JTICE.2015.01.013
40. Yildiz G, Çatalgil-Giz H, Kadirgan F (2000) Electrochemically prepared acrylamide/N, N′-methylene bisacrylamide gels. J Appl Electrochem 30:71–75. https://doi.org/10.1023/A:1003884301844/METRICS
41. Khosravi N, Youseftabar-Miri L, Divsar F et al (2022) Development and evaluation of chitosan-g-poly(acrylic acid-co-acrylamide) hydrogel composite containing gabapentin for in vitro controlled release. J Mol Struct 1270:133934. https://doi.org/10.1016/J.MOLSTRUC.2022.133934
42. Parhi R (2017) Cross-linked hydrogel for pharmaceutical applications: a review. Adv Pharm Bull 7:515. https://doi.org/10.15171/APB.2017.064

43. Jastram A, Lindner T, Luebbert C et al (2021) Swelling and diffusion in polymerized ionic liquids-based hydrogels. Polymers (Basel). https://doi.org/10.3390/POLYM13111834/S1
44. Safarzadeh H, Peighambardoust SJ, Mousavi SH et al (2022) Adsorption ability evaluation of the poly(methacrylic acid-co-acrylamide)/cloisite 30B nanocomposite hydrogel as a new adsorbent for cationic dye removal. Environ Res 212:113349. https://doi.org/10.1016/J.ENVRES.2022.113349
45. Zhao B, Jiang H, Lin Z et al (2019) Preparation of acrylamide/acrylic acid cellulose hydrogels for the adsorption of heavy metal ions. Carbohydr Polym 224:115022. https://doi.org/10.1016/J.CARBPOL.2019.115022
46. Dave PN, Kamaliya B, Macwan PM, Trivedi JH (2023) Fabrication and characterization of a gum ghatti-cl-poly(N-isopropyl acrylamide-co-acrylic acid)/CoFe2O4 nanocomposite hydrogel for metformin hydrochloride drug removal from aqueous solution. Curr Res Green Sustain Chem 6:100349. https://doi.org/10.1016/J.CRGSC.2022.100349
47. Özeroğlu C, Korkmaz Ö (2022) Synthesis and swelling behaviors of hydrogels containing LiMA groups and its use in Cu(II) adsorption from aqueous solution. Biointerface Res Appl Chem 12:3618–3637. https://doi.org/10.33263/BRIAC123.36183637
48. Islamkulov M, Karakuş S, Özeroğlu C (2023) Design artificial intelligence-based optimization and swelling behavior of novel crosslinked polymeric network hydrogels based on acrylamide-2-hydroxyethyl methacrylate and acrylamide-N-isopropylacrylamide. Colloid Polym Sci 301:259–272. https://doi.org/10.1007/S00396-023-05064-7/METRICS